Electronic Supplementary Material (ESI) for Faraday Discussions.

GPx-Mimetic Copper Vanadate Nanozyme Mediates the Release of Nitric Oxide from *S*-Nitrosothiols

*Sourav Ghosh, Punarbasu Roy, Sanjay prasad, Govindasamy Mugesh**

Department of Inorganic & Physical Chemistry, Indian Institute of Science, Bangalore 560 012; Email: mugesh@iisc.ac.in

Chemicals and materials:

All reagents used herein were of analytical grade and used directly without any further purification. Ammonium metavanadate (NH_4VO_3) was purchased from S. D. Fine Chemicals Pvt. Ltd. Hydrogen peroxide 30% (H_2O_2) was purchased from Merck. Copper (II) chloride dihydrate ($CuCl_2.2H_2O$) was purchased from Sisco Research Laboratories Pvt. Ltd. Sodium dihydrogen phosphate (NaH_2PO_4), disodium hydrogen phosphate (Na_2HPO_4), reduced glutathione (GSH), glutathione reductase (GR), D-Glucose, sodium nitrite ($NaNO_2$), Copper chloride (CuCl) were purchased from Sigma Aldrich. Copper acetate ($Cu(OAc)_2$) and 2,3-diaminonaphthalene (DAN) were purchased from Alfa Aesar. Ultrapure water was used for all the synthesis and experiments.

Characterization methods:

UV-Vis absorption spectra were recorded using SHIMADAZU UV-2600 spectrophotometer. Fluorescence spectra were acquired on HORIBA JOBIN YVON (Fluoromax-4 Spectrofluorometer). X-Ray photoelectron spectroscopy (XPS) analysis was performed on AXIS Ultra, KRATOS ANALYTICAL, SHIMADAZU. Raman spectroscopy experiments were done with Renishaw in-Via Raman Microscope (Renishaw Inc, UK). Powder XRD patterns were recorded on Phillips PANalytical diffractometer (using Cu Kα (λ = 1.5406 Å) radiation). Scanning electron microscopy (SEM) and EDX spectra were performed by using FEI Sirion UHR SEM and ESEM-Quanta instruments respectively. Transmission electron microscopy (TEM) and X-ray mapping images recorded on JEOL transmission electron microscope operating at 200 kV after casting a drop of nanoparticle dispersion in isopropyl alcohol over Cu grid. HRTEM and SAED were recorded by using Titan Themis 300kV from FEI. FT-IR spectra were acquired by PerkinElmer FT-IR spectrometer. Electron paramagnetic resonance (EPR) spectroscopy measurement were done a X-band JEOL (JES FA200) instrument. Isothermal titration calorimetry (ITC) experiments were performed by using VPITC.

Synthesis of M-oxide and M-vanadate nanomaterials:

*Synthesis of CuV_2O_6 nanowires (**CuV**)*[1]: CuV_2O_6 nanowires were synthesized using a previously reported hydrothermal route . 98 mg (0.58 mmole) of $CuCl_2.H_2O$ was dissolved in 10 mL of ultrapure water and 135 mg (1.15 mmole) of NH_4VO_3 was dissolved in another 10 mL of ultrapure water at 80°C. Once NH_4VO_3 completely dissolved, the warm solution was added slowly to the $CuCl_2$ solution under stirring resulting in the formation of a yellow precipitate. After stirring the reaction mixture for 10 min, the solution was transferred into a 30 mL Teflon-lined autoclave and heated at 210°C for 48 hours. After cooling down to room temperature, the solid product was filtered using 0.22 μM membrane filter and washed with ultrapure water and ethanol and dried at 60°C for 12 hours.

*Synthesis of ZnV_2O_6 nanowires (**ZnV**)*[2]: ZnV_2O_6 nanowires were prepared via a reported hydrothermal process. 364 mg of $Zn(NO_3)_2.6H_2O$ was dissolved in 5 mL ultrapure water and 280 mg (2.4 mmoles) of NH_4VO_3 was dissolved in another 18.5 mL of ultrapure water at 80°C. The warm NH_4VO_3 solution was

added to $Zn(NO_3)_2$ solution slowly under constant stirring. After stirring for 10 min, the solution was transferred to a 30 mL Teflon-lined autoclave and heated at 200 °C for 48 hours. After allowing the autoclaves to cool down to room temperature, white solid product was filtered using 0.22 µM membrane filters and washed with ultrapure water and ethanol then dried at 60°C for 12 hours.

*Synthesis of MnV_2O_6 nanowires (**MnV**)*[1,2]: MnV_2O_6 nanowires were synthesised by following a hydrothermal method like the ones used for CuV and ZnV. 151 mg of $Mn(NO_3)_2.4H_2O$ was dissolved in 10 mL of deionized water and 141 mg of NH_4VO_3 was dissolved in another 10 mL of ultrapure water at 80°C. Once NH_4VO_3 completely dissolved, the warm solution was added slowly to the $Mn(NO_3)_2$ solution under stirring. After stirring for 5 mins, the resultant mixture was transferred into a 30 mL Teflon-lined autoclave and heated at 210°C for 48 hours. After cooling down to room temperature, the solid product was filtered using 0.22 µM membrane filter and washed with ultrapure water and ethanol several times and dried at 60°C for 12 hours.

Synthesis of CuO nanowires: CuO nanoparticle were synthesized via standard precipitation method.[3] In 25 mL deionized water 940 mg $Cu(NO_3)_2$ was dissolved followed by addition of 25 mL NaOH (0.35 M) solution under constant stirring. The reaction mixture was stirred for 4 hours resulting in formation of blue coloured precipitate which was filtered and washed with water and dried at 60°C for 12 hours. The dried product was then calcined at 400°C for 6 hours to obtain the CuO nanoparticles.

Synthesis of Cu_2O cuboctahedron: Cu_2O cuboctahedron were synthesized by following a reported procedure with some modifications.[4] 364 mg $Cu(OAc)_2$ was dissolved in 40 mL deionized water. 10 mL of NaOH solution (3 M) was added to the reaction mixture, under constant stirring, to increase the pH. 400 mg glucose was dissolved in 10 mL deionized water which was added dropwise to the reaction mixture. The final solution was stirred at 70°C under reflux for 2 hours. After the reaction was over, the solution was cooled down to ambient temperature and the red-coloured precipitate was filtered followed by several washes with water and ethanol and then dried at 60°C for 12 hours.

Synthesis of *S*-nitrosoglutathione (GSNO):

GSNO was synthesized by following the standard method present in literature.[5] Glutathione (100 mg, 0.325 mmol) was added in 383 µL of ultrapure water followed by addition of 38 µL of concentrated hydrochloric acid. The pH of the solution was maintained between 1 and 2 and the solution was stirred in an ice bath (0-4°C). After the complete dissolution of GSH, 23 mg (0.325 mmol) of sodium nitrite was added in the solution which turned red immediately. After stirring the reaction for additional 10 min, the red colored solution was aliquoted in Eppendorf tubes and stored at -80 °C. Since GSNO is sensitive to light, the reaction was carried out in dark. Other S-nitrosothiols such as *S*-nitrosocysteine (CYSNO) was synthesized by following a similar procedure using L-cysteine.

Synthesis of Bis(*N*,*N*-diethyldithiocarbamato)iron(II) ($(dtc)_2Fe^{II}$) complex:

The $(dtc)_2Fe$ compound was synthesized following a reported procedure with minor modifications.[6,7] Briefly, $FeSO_4.7H_2O$ (217 mg, 0.78 mmol) and diethylammonium diethyldithiocarbamate (347 mg, 1.56 mmol) were added in dichloromethane (10 mL) and the reaction mixture was stirred for 8 h. The resultant brown solution was filtered, and the brown filtrate was dried under reduced pressure to obtain $(dtc)_2Fe^{II}$ as a brown solid, which was then recrystallized in diethyl ether to get pure $(dtc)_2Fe^{II}$.

Catalase (CAT)-like activity assay:

CAT-like activity of CuV and other nanomaterials were checked by monitoring the absorbance of H_2O_2 at 240 nm (ε_{240} = 39.4 M^{-1} cm^{-1})[8] using UV-vis spectrophotometer. Assay conditions: 10 mM H_2O_2, 5 ng μL^{-1} nanomaterial. Total reaction volume = 1 mL. A control reaction was carried out in the absence of nanomaterials where MnO_2 (commercial) was used as a positive control as it is known to have CAT-like activity. Presence of nanomaterials did not result in significant decrease in the absorbance at 240 nm indicating that none of the materials had CAT-like activity.

Superoxide dismutase (SOD)-like activity assay:

SOD mimetic activity of CuV was checked by using a dye, WST-1 (2-(4-Iodophenyl)-3-(4-nitrophenyl)-5-(2,4-disulfophenyl)-2H-tetrazolium) coupled with xanthine/xanthine oxidase (XO) where superoxide ($O_2^{\cdot-}$) generated in the reaction of xanthine/xanthine oxidase, can reduce WST-1 to spectrophotometrically detectable formazan at 440 nm using 96 well plate.[8,16]The percentage of formazan production is proportional to the amount of superoxide anions generated in the reaction mixture, and therefore, the SOD-like activity of nanoparticles can be quantified by measuring the decrease in the formazan production.

Co-operativity of CuV nanozyme to work in a cascade:

To study the cooperativity of CuV nanozymes with other enzymes, we introduced glucose oxidase enzymatic cycle with GR-coupled GPx cycle to generate *in-situ* H_2O_2. Briefly, the glucose oxidase (0.25 U) was incubated with glucose (250 mM) for 2 min. After that other reagents were added into the reactive mixture required for the GPx-like activity and the decrease in the absorbance of NADPH was monitored at 340 nm spectrophotometrically. From the decrease of the absorbance of NADPH, initial rates were calculated.

Table S1. Molar extinction coefficients (ε) of S-nitrosothiols at 335 nm.[8,9]

S-nitrosothiol	Molar Extinction Coefficient (mM^{-1} cm^{-1})
SNAP	1.00
GSNO	0.85
CYSNO	0.74

Table S2. Frequences and g-values obtained from the EPR-spectra

NO-source	NO-complex	Frequency (MHz)	g-value
[10]GSNO	$(dtc)_2FeNO$	9453.4	g1=2.018, g2=2.008, g3=2.002
GSNO + GSH		9453.4	g1=2.018, g2=2.008, g3=2.003
GSNO + CuV		9450.1	g1=2.018, g2=2.010, g3=2.002
GSNO + CuV + GSH		9450.6	g1=2.018, g2=2.010, g3=2.002

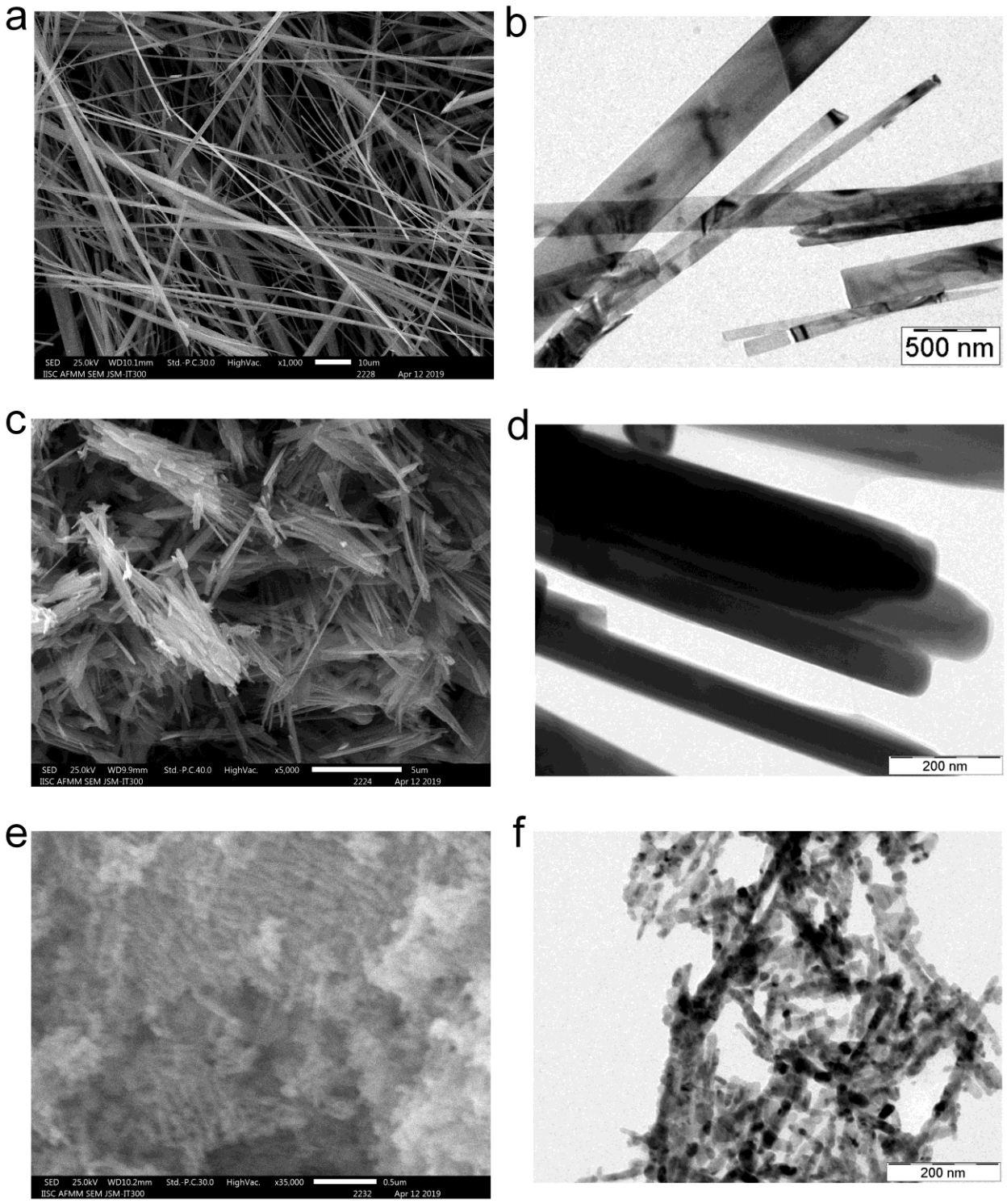

Figure S1. SEM images of a) ZnV, c) MnV and e) CuO respectively. TEM images of b) ZnV, d) MnV and f) CuO respectively. The images confirm wire-like morphology of all the materials. The SEM and TEM images reveal that the average length and diameter of vanadates are 1-2 μm and 150-250 nm respectively.

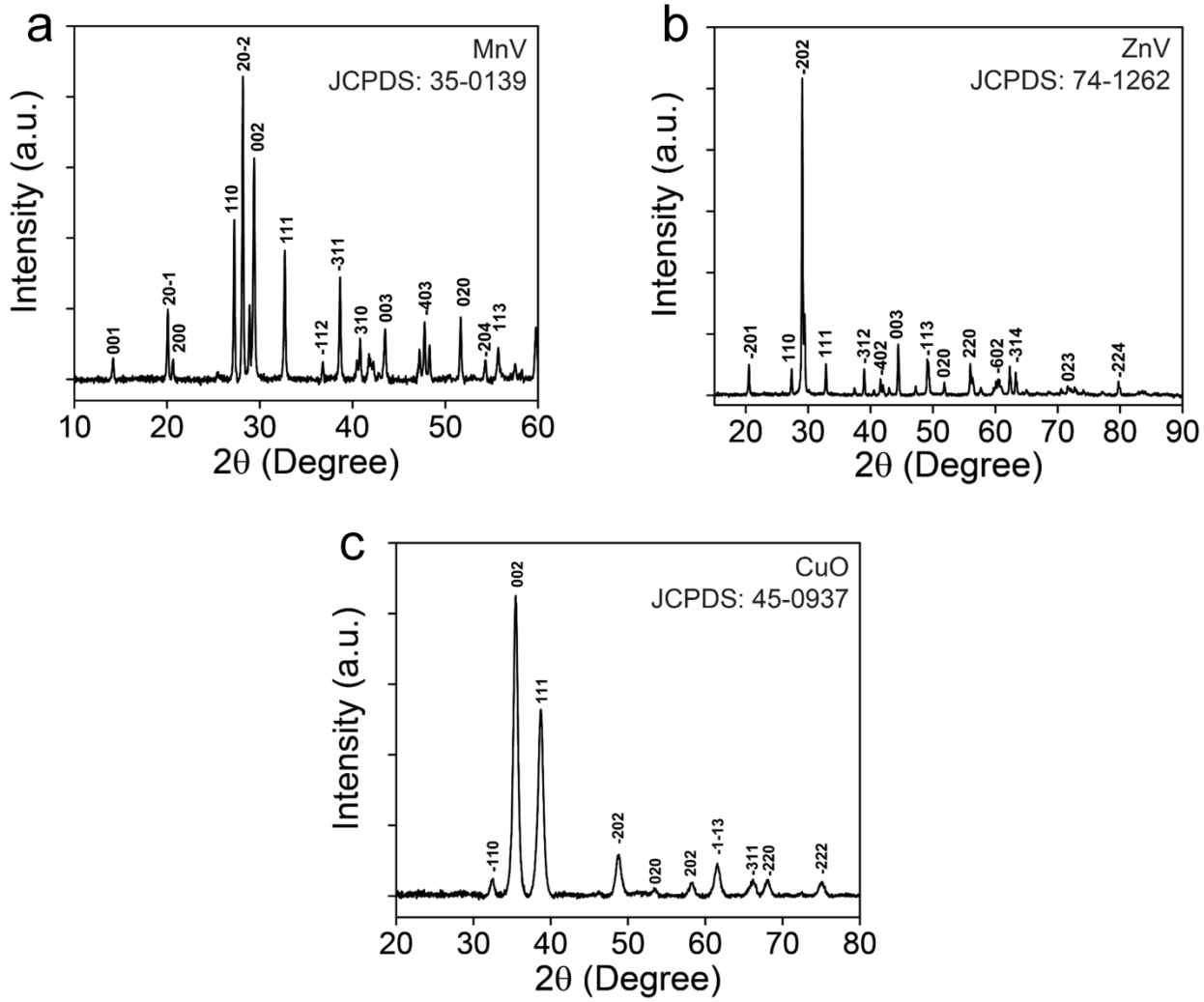

Figure S2. Powder X-ray diffraction of a) MnV_2O_6 (MnV), b) ZnV_2O_6 (ZnV) and c) CuO. The sharp peaks in PXRD indicate the crystalline nature of the materials. All peaks were matched with the standard JCPDS pattern of monoclinic phase.

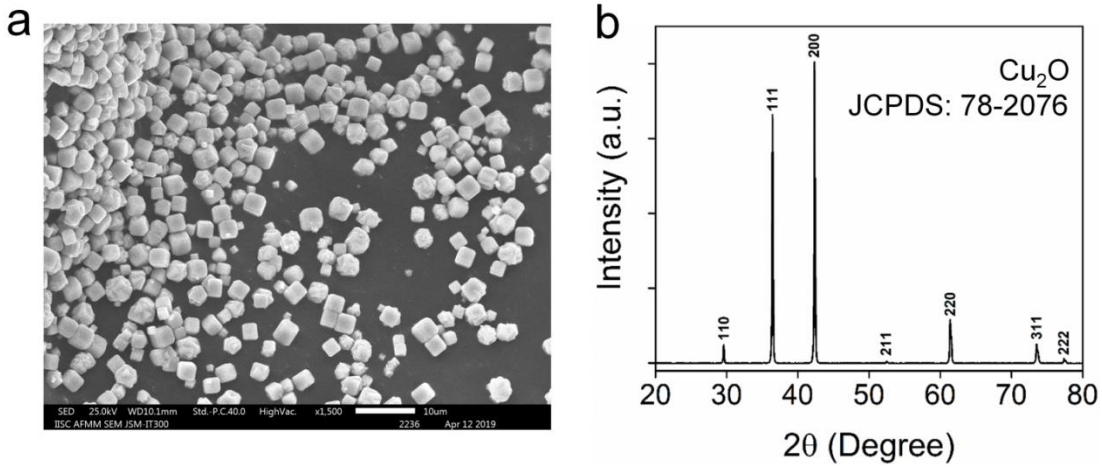

Figure S3. Characterization of Cu_2O nanomaterial. a) SEM images showing cuboctahedron morphology of Cu_2O. b) PXRD pattern of Cu_2O. The sharp peaks indicate the crystallinity of Cu_2O. The PXRD pattern of Cu_2O was indexed to the standard cubic fcc structure.

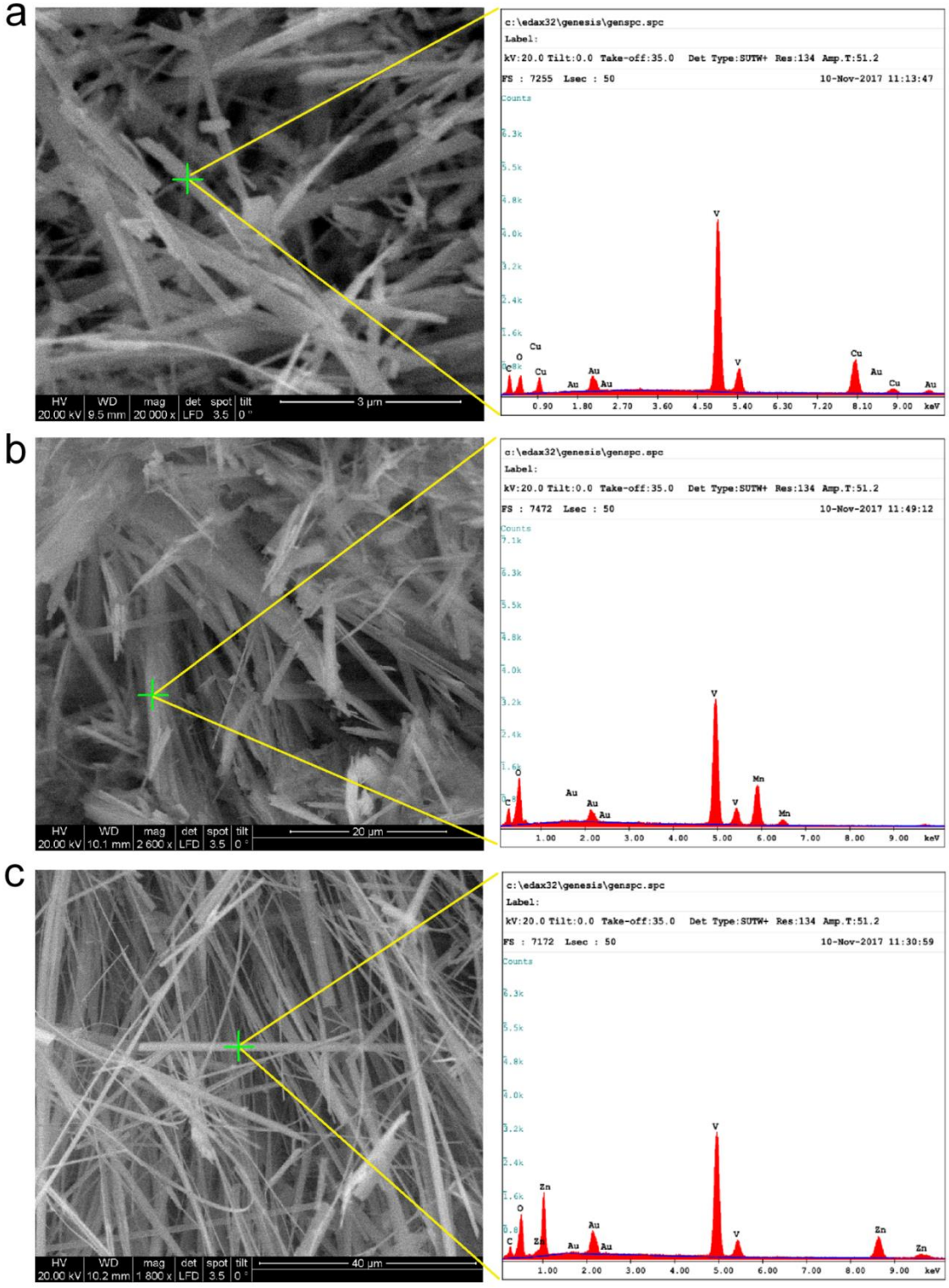

Figure S4. EDS spectra (right column) of metal vanadate nanomaterials. a) CuV, b) MnV c) ZnV. EDS spectra were recorded at the region marked by the green crosshair in the SEM images (left column). Small peak at ~2.0 KeV was due to the Au coating of the samples and carbon peak was due to the atmospheric carbon.

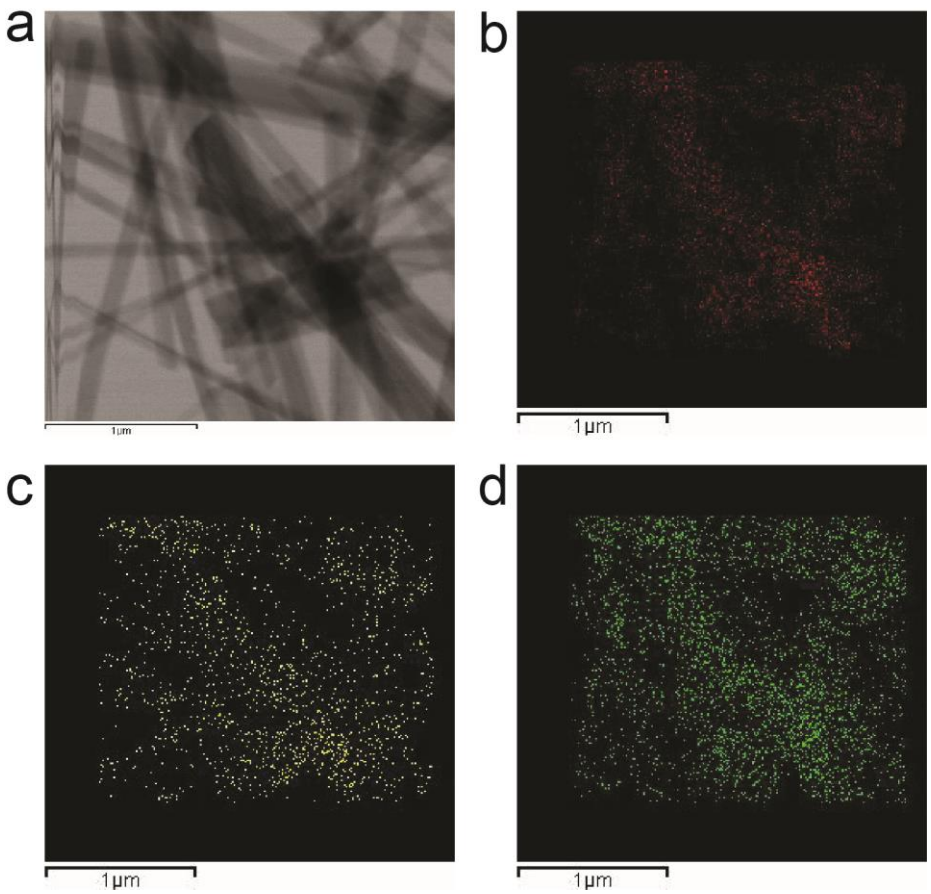

Figure S5. X-ray mapping images of CuV nanomaterials. a) Selected area bright field (SABF) image, b-d) distribution of V, O and Cu atoms, respectively.

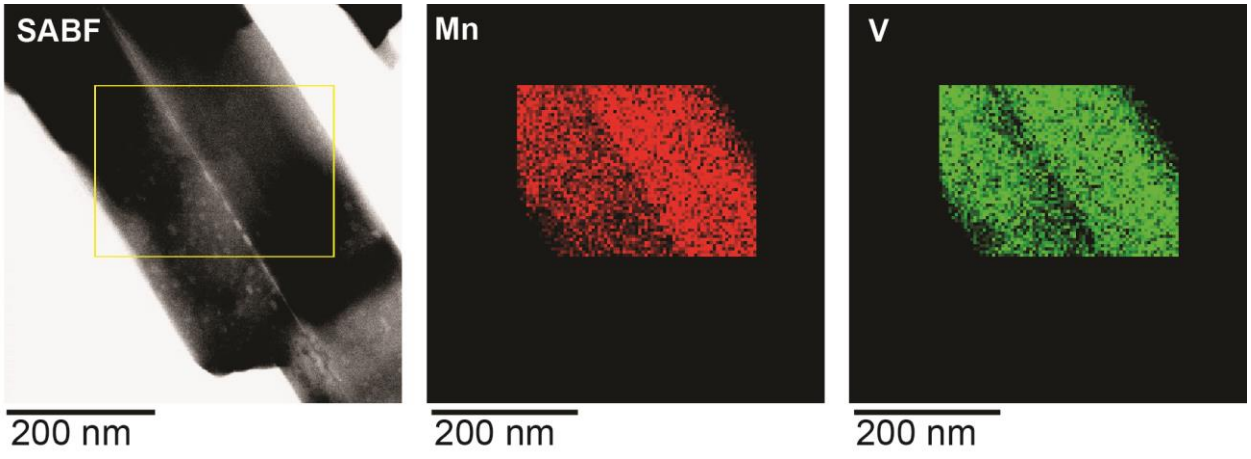

Figure S6. X-ray mapping images of MnV. Selected area bright field (SABF) image (left), distribution of Mn atoms (middle), and V atoms (right).

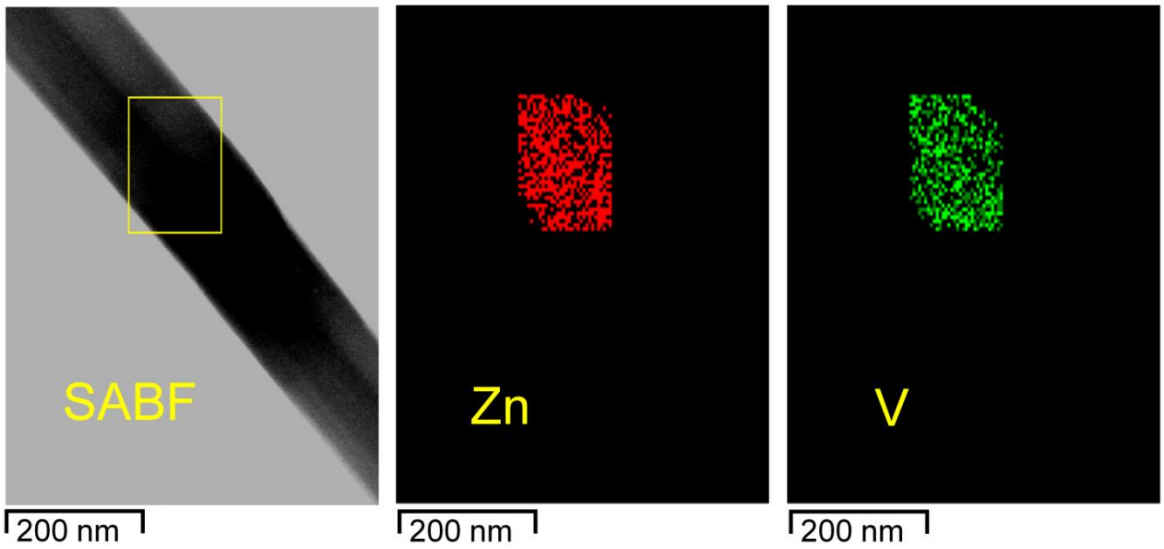

Figure S7. X-ray mapping images of ZnV. Selected area bright field (SABF) image (left), distribution of Zn atoms (middle), and V atoms (right).

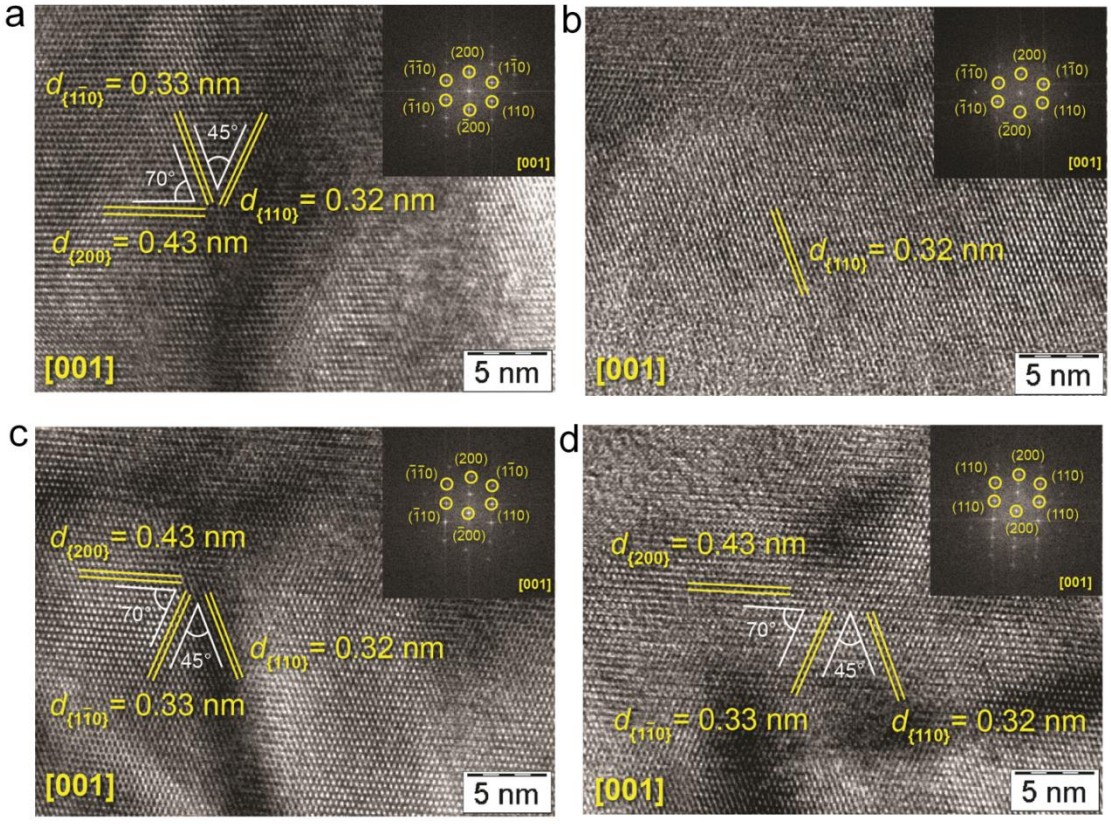

Figure S8. a-d) HRTEM images and their corresponding Fast-Fourier-Transform (FFT) patterns (index) of CuV. The FFT patterns were indexed along [001] zone axis. The lattice fringes observed in HRTEM are (1-10), (110) and (200) planes with d-spacing of 0.33 nm, 0.32 nm and 0.43 nm respectively. The interfacial angle of (1-10) and (110) is 45.0º, similarly the interfacial angle between (200) and (1-10) is 70.0°. These three planes in the HRTEM fall in the common zone axis [001].

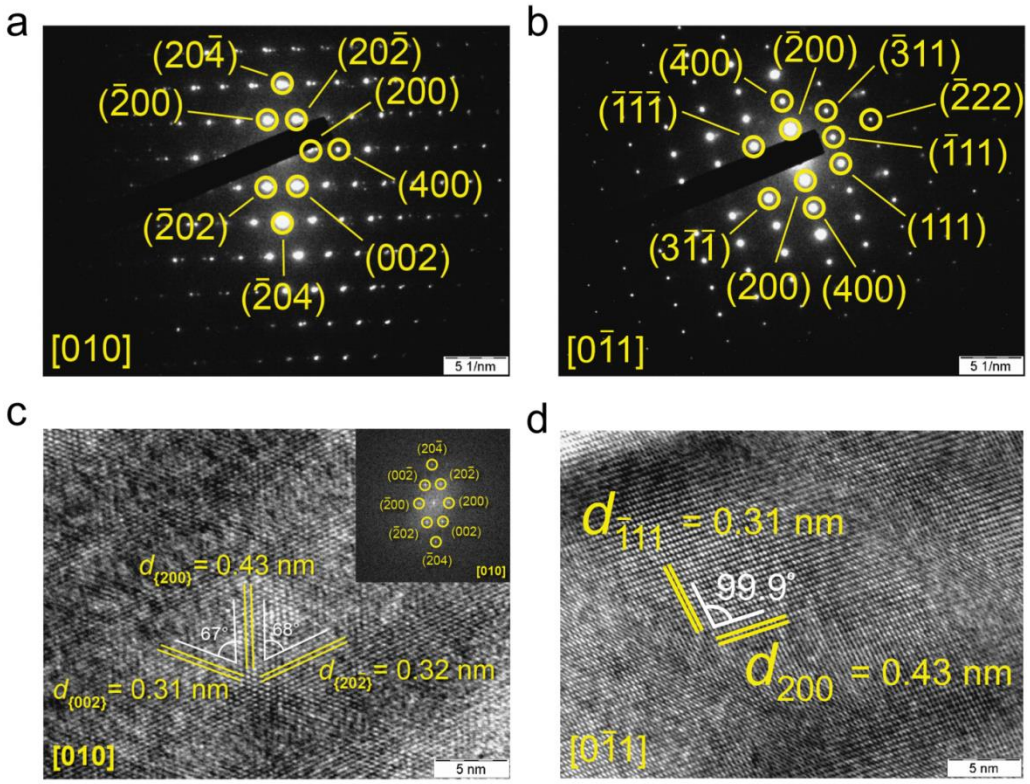

Figure S9. a, b) Selected area electron difrraction (SAED) patterns of MnV and ZnV, respectively. g, h) HRTEM images of MnV and ZnV, respectively. The well defined bright spots in SAED and well resolved lattice frienges in HRTEM images confirms that the synthesized materials are highly crystaline in nature. After analysing the SAED and HRTEM, the Zone axis were assigned as [010] and [0-11] for MnV and ZnV respectively.

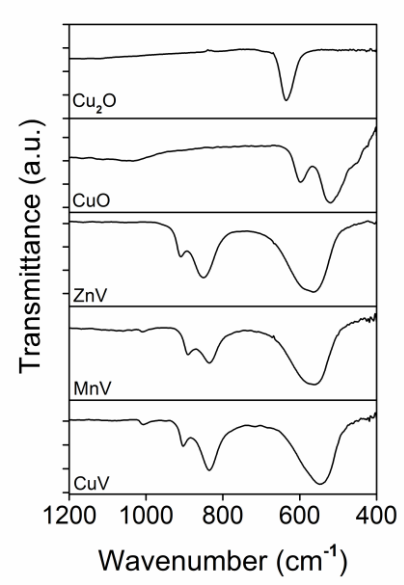

Figure S10. FT-IR spectra of (400 cm^{-1} to 1200 cm^{-1}) nanomaterials where metal oxides show most of the vibrational characteristics peak of M-O bonds. The peaks in the range of 800-1000 cm^{-1} are due to V-O asymmetric stretching and bending vibrations. The peak at bellow 600 cm^{-1} is due to the M-O stretching / V-O-V symmetric stretching in MV_2O_6.[13-17] The peak at 535 and 565 cm^{-1} is due to the vibration of Cu^{II}-O. The peak at 635 cm^{-1} is characteristic of Cu^{I}-O stretching vibration.

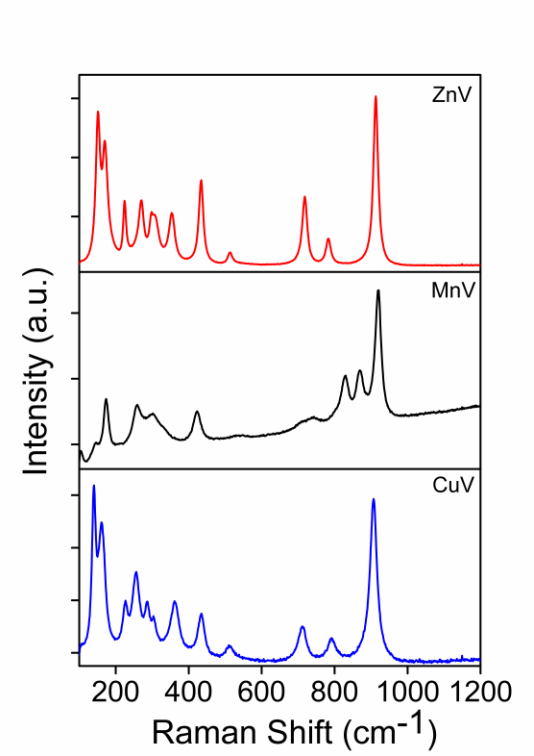

Figure S11. FT-Raman spectra of three metal vanadate. The peak bellow 700 cm^{-1} i.e. at 905, 790, and 714 cm^{-1} are assigned to the stretching vibrations of the V-O1, V-O2, and V-O3 bonds, respectively. The Raman bands located in the region of 600–200 cm^{-1} are due to the M-O modes and the V-O bending vibrations in MV_2O_6. The remaining two bands below 200 cm^{-1} are assigned to the lattice vibrations.[11,12]

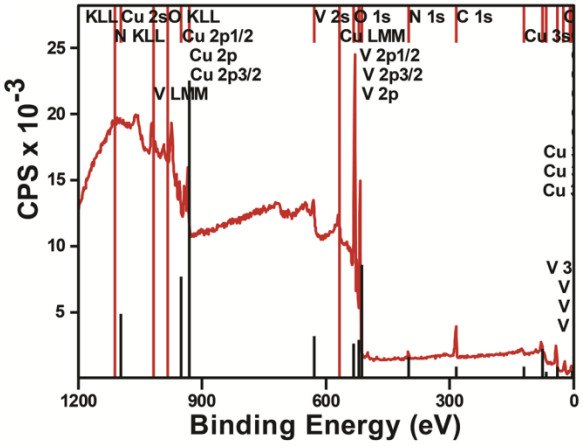

Figure S12. Wide range X-ray photoelectron spectrum of CuV. No impurity peaks except C and N were identified confirm the elemental purity of the material. The C and N peaks in the wide XPS probably came from atmospheric CO_2 and N_2.

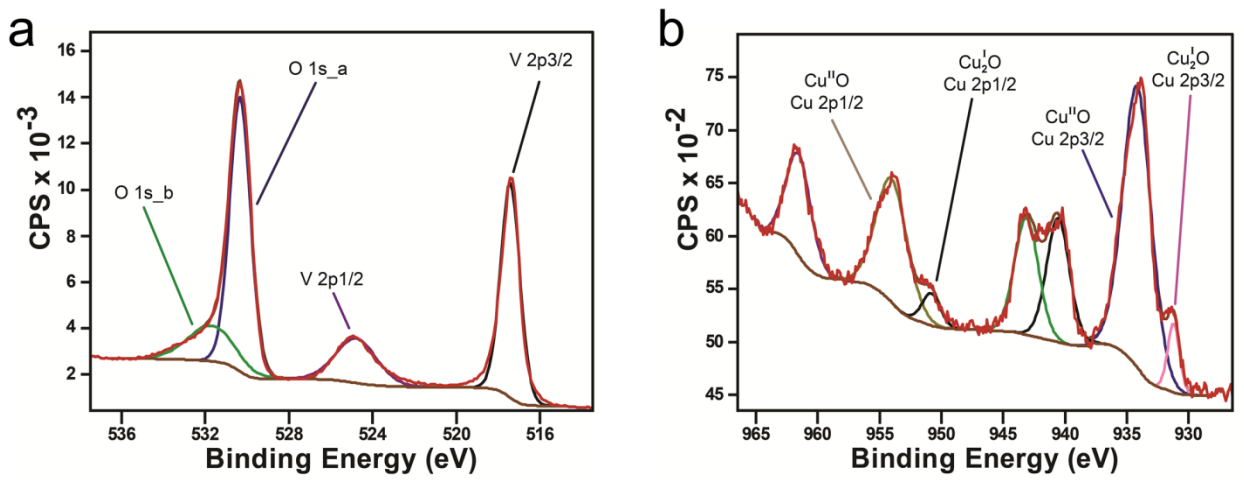

Figure S13. Narrow range XPS of CuV showing peak for a) oxygen and vanadium, b) copper. The spectra were calibrated by taking C1s (284.6 eV) as a standard. Binding energy values confirm the +5 oxidation state of vanadium and +2 oxidation state of copper in CuV. The small peaks observed at 931.22 (Cu $2p_{3/2}$), and 950.82 (Cu $2p_{1/2}$) in the deconvoluted spectra of Cu was assigned to +1 state of Cu which is present as small impurity along with Cu^{II} on the surface of CuV.

Table S3. Binding energies and full width at half maxima (FWHM) of CuV obtained from XPS.[1,10,14-18]

CuV	Binding Energy (eV)	FWHM
Cu (I) $2p_{3/2}$	931.22	1.12
Cu (I) $2p_{1/2}$	950.82	1.7
Cu (II) $2p_{3/2}$	934.16	2.69
Cu (II) $2p_{1/2}$	954.01	2.93
O 1s_a	530.33	1.15
O 1s_b	531.69	2.64
V $2p_{3/2}$	517.12	1.07
V $2p_{1/2}$	524.78	2.28

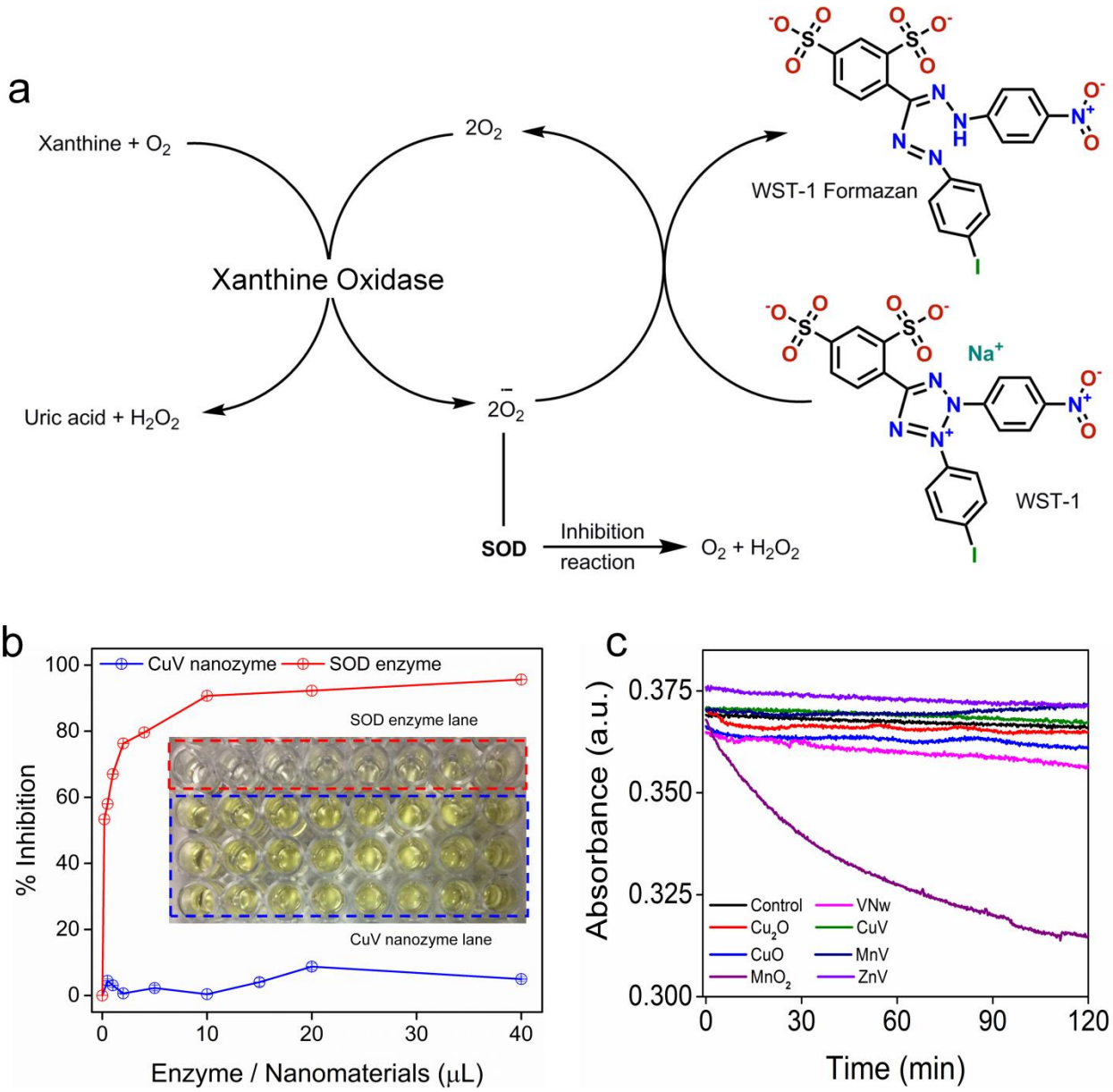

Figure S14. a) Schemetic representation of superoxide dismutase (SOD) enzymatic assay.[19,20] SOD mimetic activity of CuV was checked by using a dye, WST-1 (2-(4-Iodophenyl)-3-(4-nitrophenyl)-5-(2,4-disulfophenyl)-2H-tetrazolium) coupled with xanthine/xanthine oxidase (XO) where superoxide (O_2^-) generated in the reaction of xanthine/xanthine oxidase, can reduce WST-1 to spectrophotometrically detectable formazan at 440 nm. b) Graph shows the % of SOD activity measured from the percentage of formazan production which is proportional to the amount of superoxide anions generated in the reaction mixture. Inset shows the lanes where SOD enzyme was used as +ve control. The yellow coloration implies the formation of more amount of formazan. In the CuV lanes intense yellow color was observed which confirmed that the material did not have SOD-like activity. In SOD enzyme lanes, with increasing the concentration of enzyme (60 ng.μL^{-1}) there was a gradual decrease of yellow coloration was noticed affirmed scavenging of superoxide radicals by SOD. c) Comparisons of catalase like activity[20] of different nanomaterials. Assay condition: sodium phosphate buffer pH = 7.4, Catalyst = 5 ng μL^{-1}; H_2O_2 = 10.0 mM, Temp. = 25 ^{0}C. Except MnO_2, which is known to be catalase mimic, no other material showed catalase like activity.

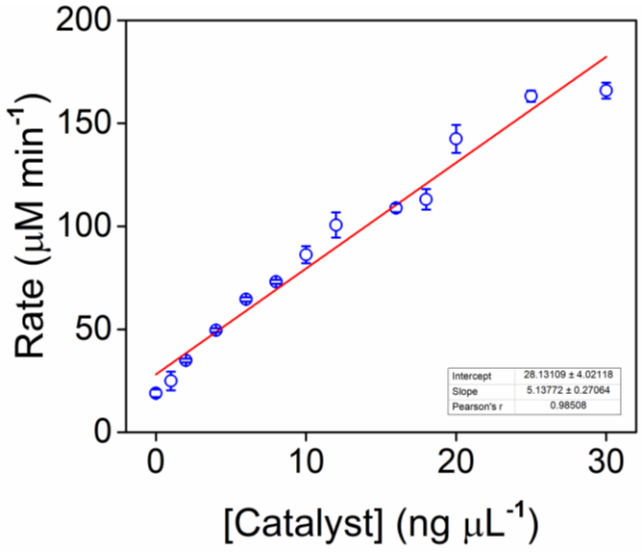

Figure S15. Initial rate of the reaction vs catalyst concentrations. Assay conditions: CuV (0-30 ng μL^{-1}), NADPH (0.2 mM), GSH (2 mM), GR (~1.7 units), H_2O_2 (0.2 mM) in phosphate buffer (100 mM, pH 7.4), 25 °C.

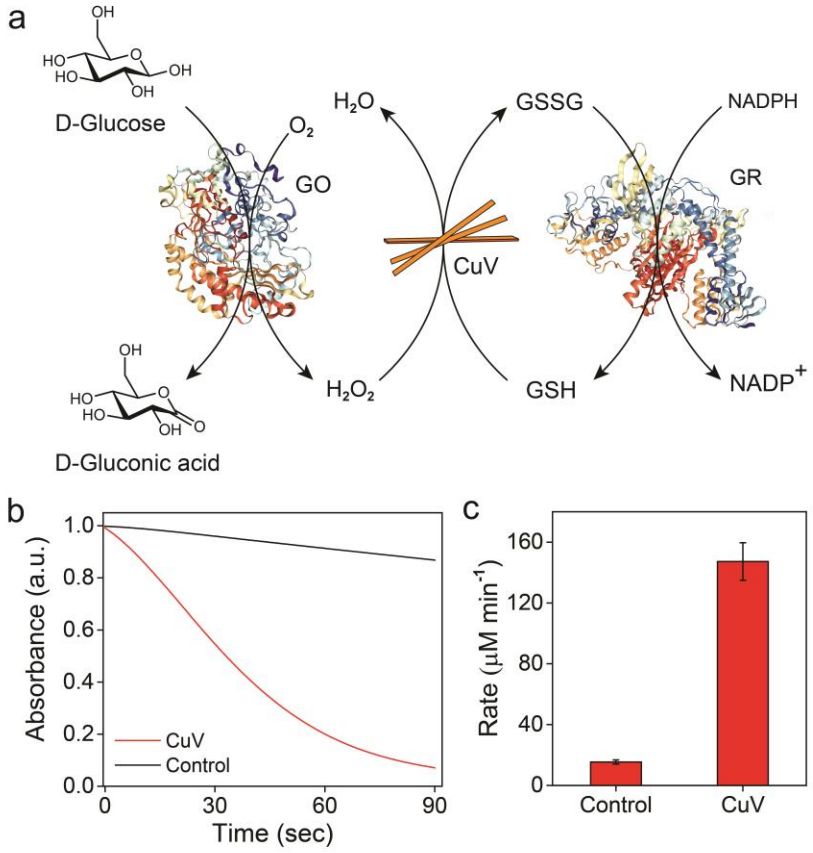

Figure S16. Cooperativity of CuV nanozymes with glucose oxidase (GO) to work in a cascade. a) Schematic representation of the *in-situ* generation of H_2O_2 by glucose oxidase (GO), using glucose, which is further used in catalysis by CuV nanozymes. b) Absorbance versus time (sec) plot for GPx activity assay using *in-situ* generated. H_2O_2 by CuV. The decrease of absorbance was monitored at 340 nm. c) Bar diagram showing the comparison of initial rates of CuV with respect to control (without nanomaterial). The result indicates CuV takes *in-situ* generated H_2O_2 for the catalysis.

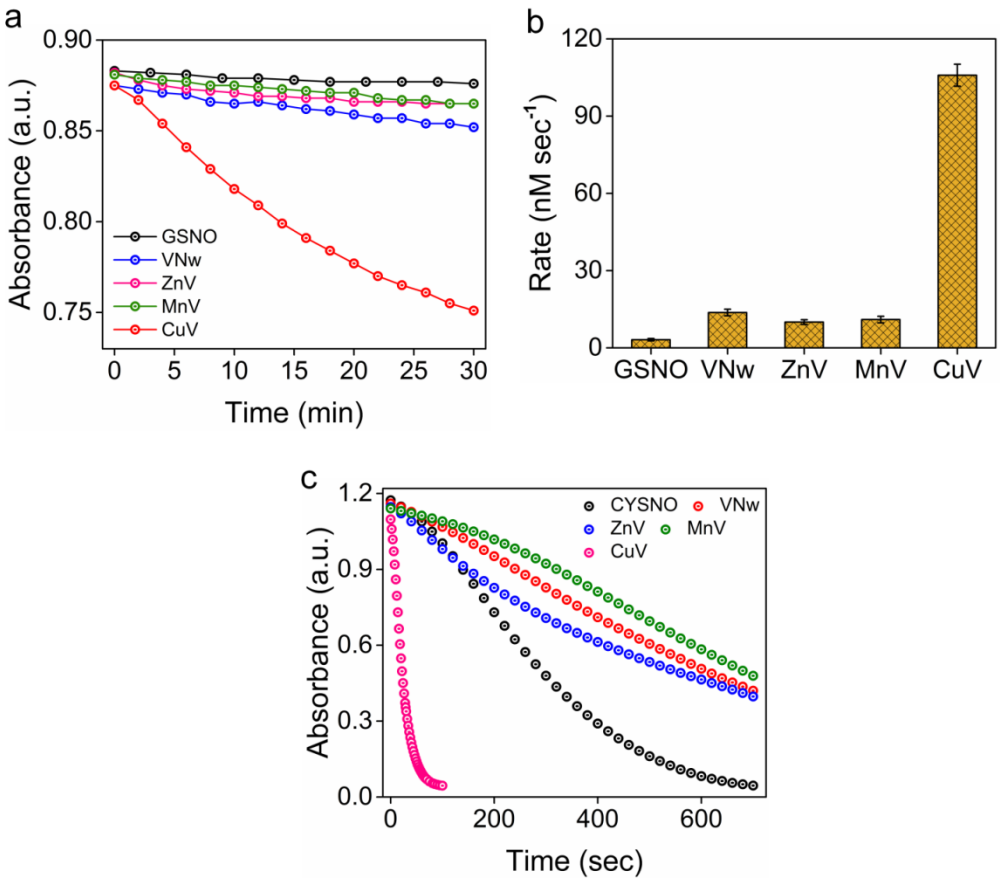

Figure S17. De-nitrosylation of RSNO by different M-oxide nanomaterials. a) The decrease in the absorbance of GSNO was monitored at 335 nm by UV-Vis spectrophotometer. Assay condition: GSNO (1.0 mM), catalyst (20 ng μL^{-1}), 0.1 M sodium phosphate buffer (pH 7.4), 25 °C. b) Bar diagram shows the comparison of the rate of denitrosylation of GSNO by different nanomaterials. c) The decrease in the absorbance of CYSNO was monitored at 335 nm by UV-Vis spectrophotometer. Assay condition: CYSNO (1.5 mM), catalyst (0.4 ng μL^{-1}), 0.1 M sodium phosphate buffer (pH 7.4), 25 °C.

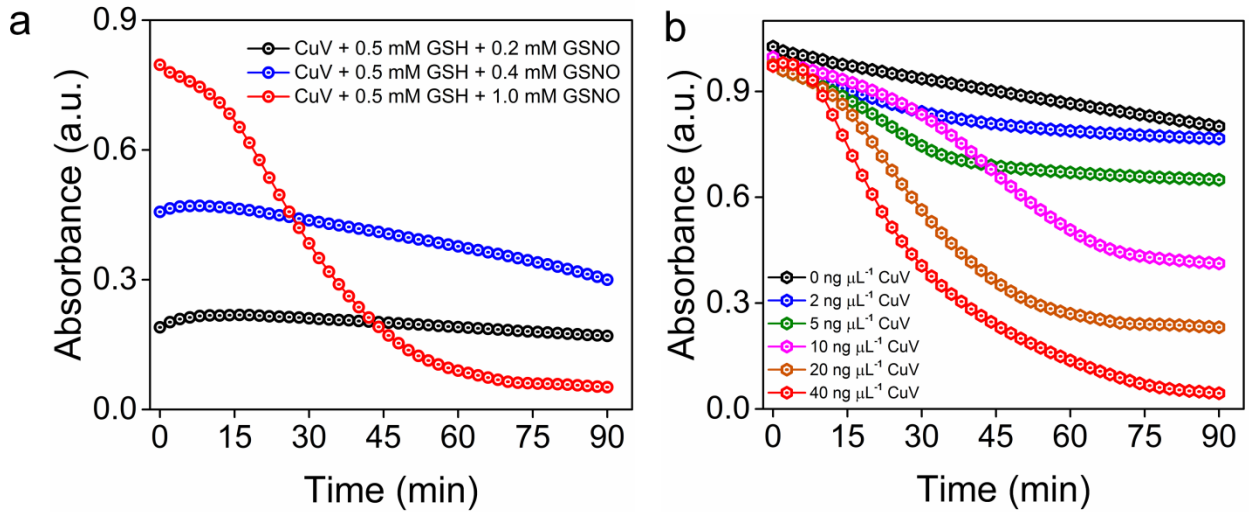

Figure S18. a) Denitrosylation reaction by CuV with varying concentration of GSNO. Assay condition: GSNO (0.2 - 1.0 mM), catalyst (20 ng μL^{-1}), GSH (0.5 mM), 0.1 M sodium phosphate buffer (pH 7.4), 25 °C. b) Denitrosylation of GSNO with varying concentration of CuV. Assay condition: GSNO (1.0 mM), catalyst (0 - 40 ng μL^{-1}), GSH (0.5 mM), 0.1 M sodium phosphate buffer (pH 7.4), 25 °C.

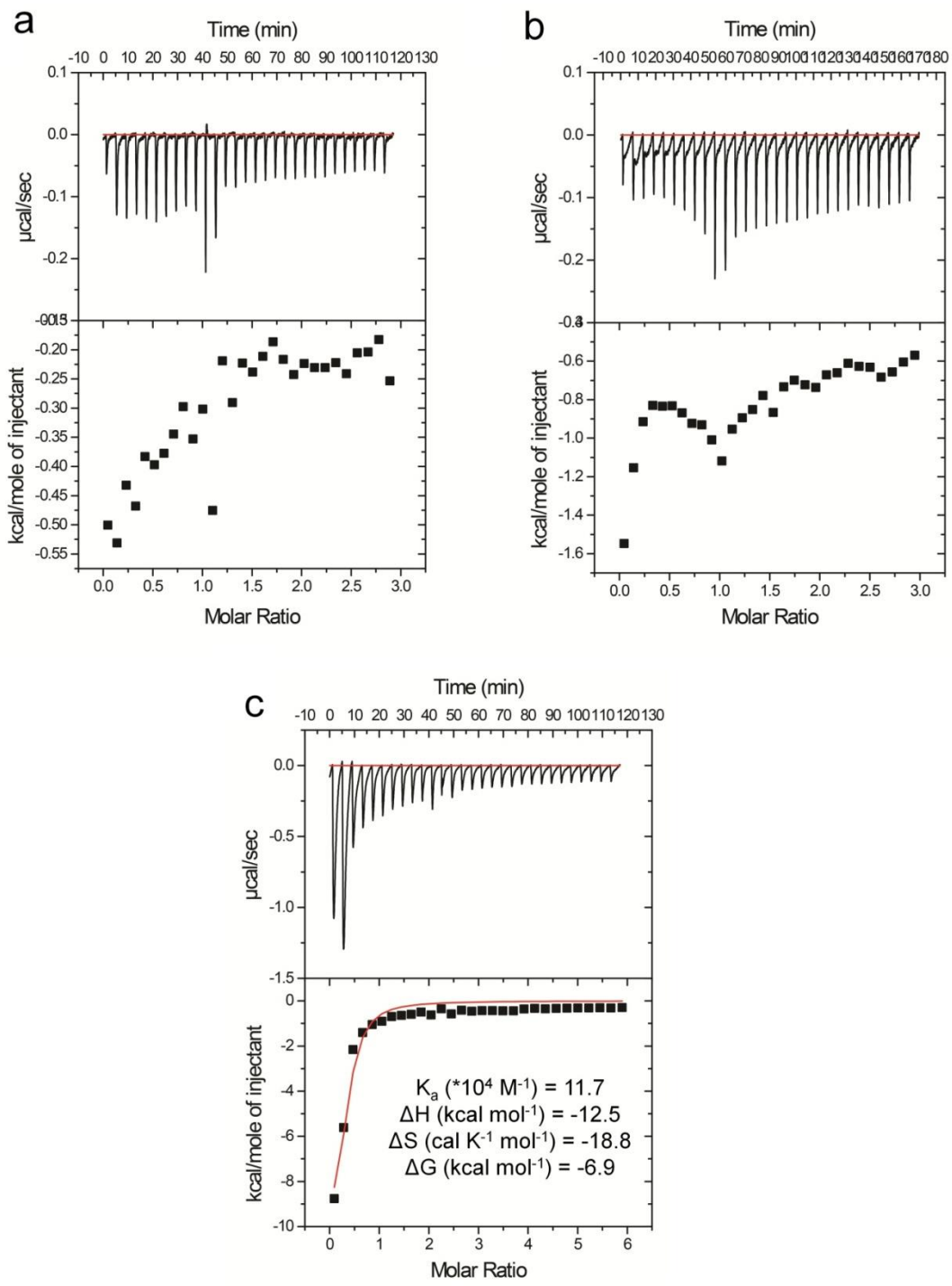

Figure S19. Isothermal titration calorimetry (ITC) profile for binding of GSH at 298 K. a) Without catalyst and GSH (1.0 mM), b) VNw (20 ng μl^{-1}) with 1.0 mM GSH and c) CuV ((20 ng μl^{-1} or 0.075 mM, considering molar mass of CuV as 261.43 g mol^{-1}) with 2.0 mM GSH. The original titration profile (top) and the integrated heat (bottom) of each reaction are shown. Thermodynamic parameters shown in c) for CuV, were obtained using one-site binding model.

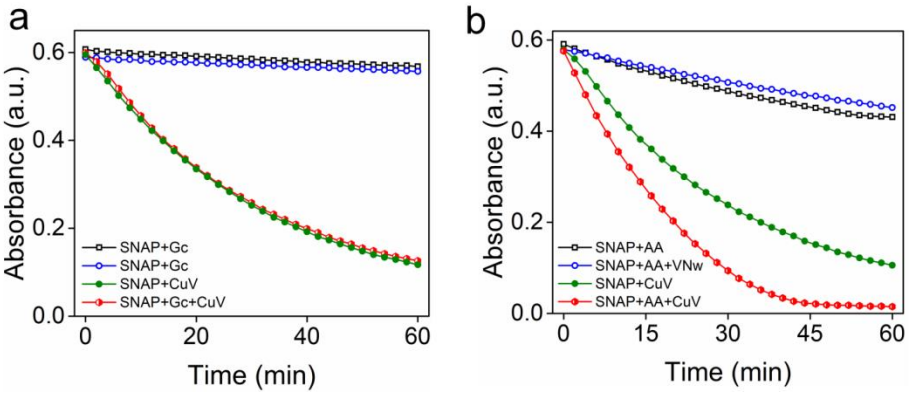

Figure S20. a) Denitrosylation of SNAP by CuV in presence of reducing agents a) glucose (Gc) b)ascorbic acid (AA). Assay condition for a) : SNAP (0.5 mM), catalyst (4 ng μL^{-1}), glucose (0.5 mM), 0.1 M sodium phosphate buffer (pH 7.4), 25 °C. As glucose is mild reducing agent there was no difference in denitrosylation was observed between the conditions (SNAP+CuV) and (SNAP+CuV+Gc). Assay condition for b) : SNAP (0.5 mM), catalyst (4 ng μL^{-1}), ascorbic acid (0.005 mM), 0.1 M sodium phosphate buffer (pH 7.4), 25 °C. The difference in the rate of denitrosylation was observed between the conditions (SNAP+CuV) and (SNAP+CuV+AA) indicates ascorbic acid was capable of reducing Cu^{+2} to Cu^{+1} species on the surface of CuV.

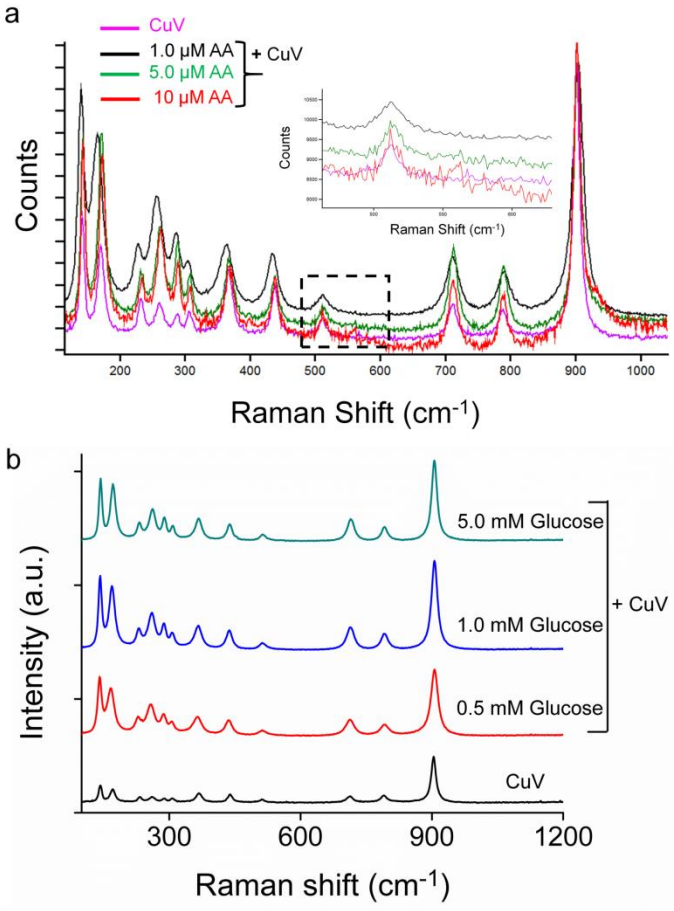

Figure S21. a) FT-Raman spectra of CuV after reaction with varying concentration of ascorbic acid (AA). The small peak observed at ~550 cm^{-1} (along with 12 peaks of parent CuV) at higher concentration of AA treatment is due to the formation of Cu^{I} species on the surface of CuV.[11,14-17] b) FT-Raman spectra of CuV after reaction with varying concentration of glucose (Gc). No additional peak was observed even at higher concentration of Gc treatment indicating Gc is very mild reducing agents and not capable of forming Cu^{I} species from Cu^{II} on the surface of CuV. As ascorbic acid and glucose concentration in human blood is ~3 μM and ~1.0 mM respectively. Here we used the concentration of AA in the micromolar range and of glucose in the milimolar range.

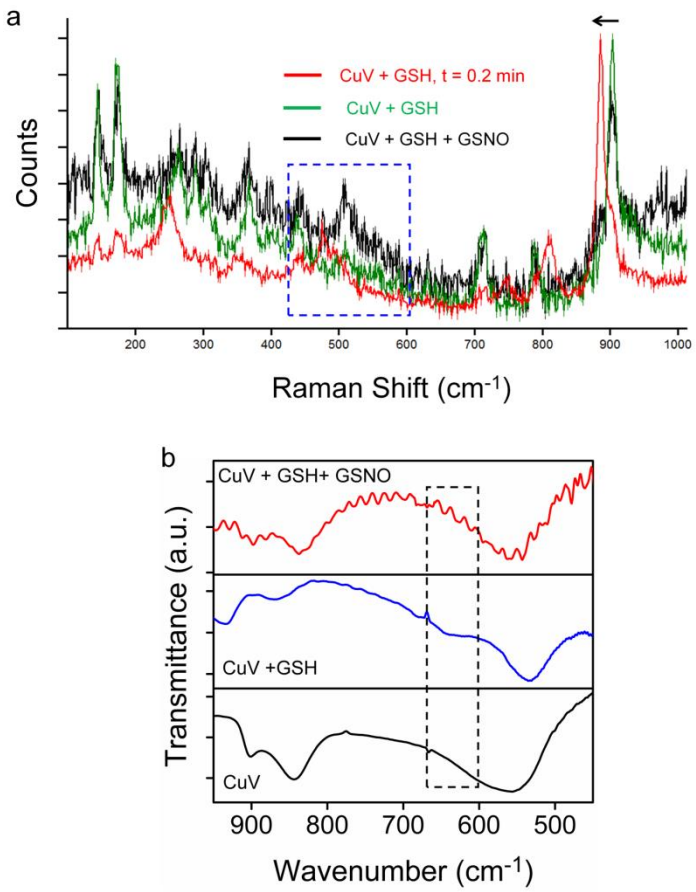

Figure S22. a) FT-Raman spectra of CuV during denitrosylation of GSNO in presence of GSH (1 mM). The red spectrum was taken after immediate treatment of GSH. The peak observed at 481 cm^{-1} corresponds to $Cu(OH)_2$ species on the surface. The peak at 905 cm^{-1} (V=O) is little shifted towards lower wavenumber indicates the interaction of GSH with V=O. The green spectrum was recorded afterwards where small peak observed at ~550 cm^{-1} is due to the formation of Cu^{I} species upon reduction of Cu^{II} species by GSH. [11,14-17] After complete denitrosylation of GSNO 12 signature peaks of CuV was observed (black spectrum) indicates the suffling between Cu^{II} and Cu^{I} is responsible for denitrosylation activity of CuV. Similar results were obtained while recording b) FT-IR spectra.[13-17] of CuV during denitrosylation of GSNO in presence of GSH (1 mM). The small broad peak observed at 635 cm^{-1} (characteristic of Cu^{I}–O vibration) when CuV was reacted with GSH (Blue spectrum). After complete denitrosylation of GSNO, the peak at 635 cm^{-1} disappeared correlating well with the previous observation in FT-Raman spectra.

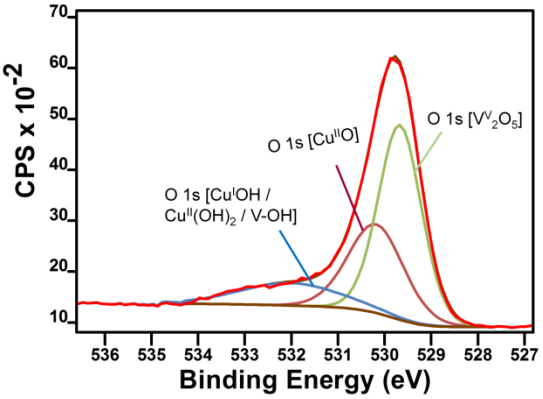

Figure S23. Narrow range XPS of O1s after treatment of CuV with ascorbic acid (5 µM). The peaks are deconvoluted and assigned according to binding energies and FWHM. The binding energy of C1s (284.6 eV) was used as standard to calibrate the spectra.

Table S4. Binding energies and full width at half maxima (FWHM) of O 1s obtained from XPS.[1]

CuV (O 1s)	Binding Energy (eV)	FWHM
O 1s (V_2O_5)	529.67	1.08
O 1s (CuO)	530.18	1.40
O 1s (M-OH)	532.02	2.56

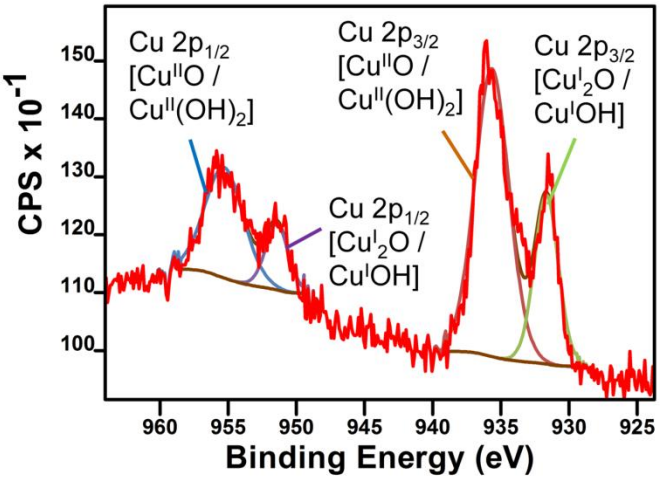

Figure S24. Narrow range XPS of Cu 2p after treatment of CuV with GSH (10 mM). The peaks are deconvoluted and assigned according to binding energies and FWHM. The binding energy of C1s (284.6 eV) was used as standard to calibrate the spectra.

Table S5. Binding energies and full width at half maxima (FWHM) of Cu 2p obtained from XPS.[1,14-17]

CuV (Cu 2p)	Binding Energy (eV)	FWHM
Cu (I) $2p_{3/2}$	931.67	2.07
Cu (I) $2p_{1/2}$	951.42	1.95
Cu (II) $2p_{3/2}$	935.66	2.92
Cu (II) $2p_{1/2}$	955.29	3.31

Table S6. Binding energies and full width at half maxima (FWHM) of S 2p obtained from XPS.[21-23]

CuV (S 2p)	Binding Energy (eV)	FWHM
Cu_2S	161.67	0.88
CuS	162.81	1.20
-SH / -S-S-	164.16	2.05
$-SO_2H$ / $-SO_3H$	167.20	2.67

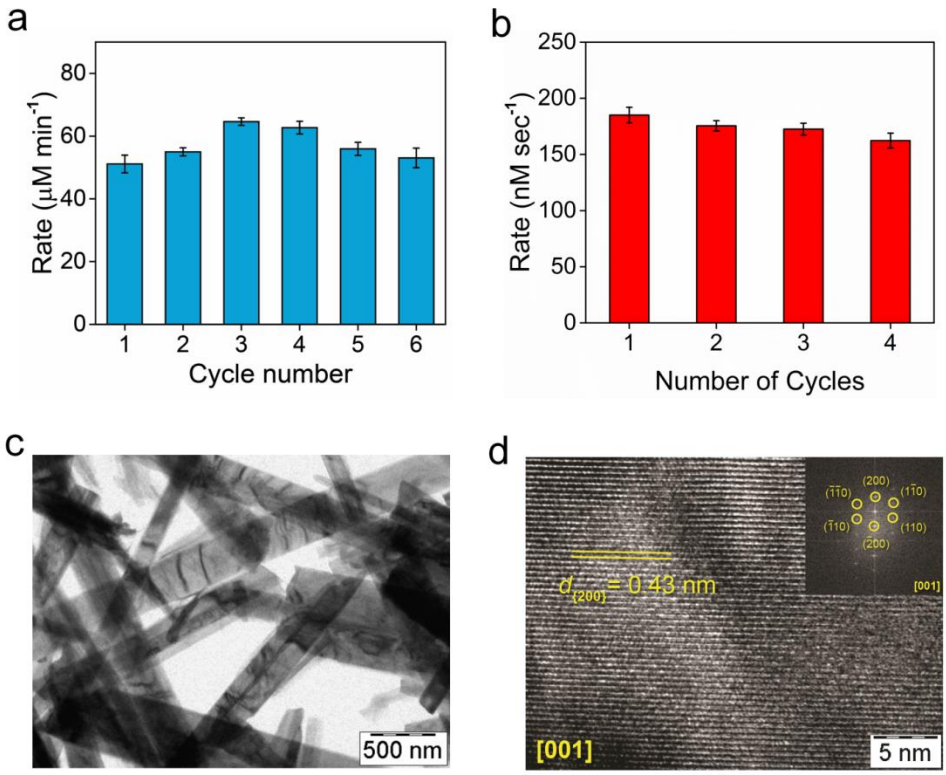

Figure S25. a) Recyclability of CuV during catalysis analysed by addition of fresh substrate (H_2O_2) in the reaction mixture up to six cycles. Bar diagram showing the initial rate for each cycles of catalysis. Conditions used for the assay was sodium phosphate buffer (100 mM, pH 7.4), GSH (2 mM), NADPH (0.4 mM), catalyst (20 ng μL^{-1}), GR (~1.7 U) and H_2O_2 (25 μM) at 25 ºC. The comparable initial rates among multiple cycles depicted the stability and robustness of the catalyst. b) Bar diagram demonstrating the recyclability of CuV (20 ng μL^{-1}) upto four cycles of and rate of denitrosylation using 0.5 mM GSNO in each cycle along with 0.25 mM GSH in 0.1 M phosphate buffer (pH 7.4) at 25 °C. No significant change in the initial rate of de-nitrosylation was observed as the nanomaterials retained their activity throughout multiple cycles. c,d) TEM and HRTEM images respectively after catalysis (GPx) showing the morphology and the planes are intact after catalysis.

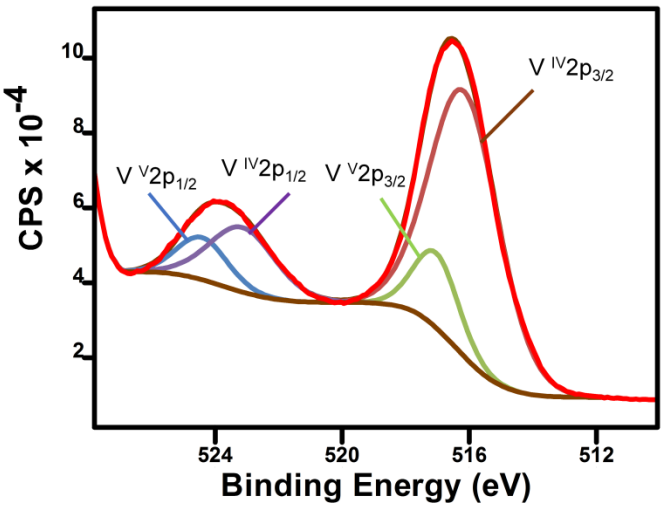

Figure S26. Narrow range XPS of V 2p after catalysis (GPx-like) and followed by treatment of excess (0.1 M) H_2O_2. The peaks are deconvoluted and assigned according to binding energies and FWHM. The binding energy of C1s (284.6 eV) was used as standard to calibrate the spectra. Vanadium oxidation state were identified as both +5 and +4 in the spectra indicated the GPx-like activity by CuV is occuring through the redox change of vanadium center.

Table S7. Binding energies and full width at half maxima (FWHM) of V 2p obtained from XPS after catalysis.[1,15,24]

CuV (V 2p)	Binding Energy (eV)	FWHM
V (IV) $2p_{3/2}$	516.14	2.53
V (IV) $2p_{1/2}$	523.13	2.44
V (V) $2p_{3/2}$	517.03	1.66
V (V) $2p_{1/2}$	524.40	1.87

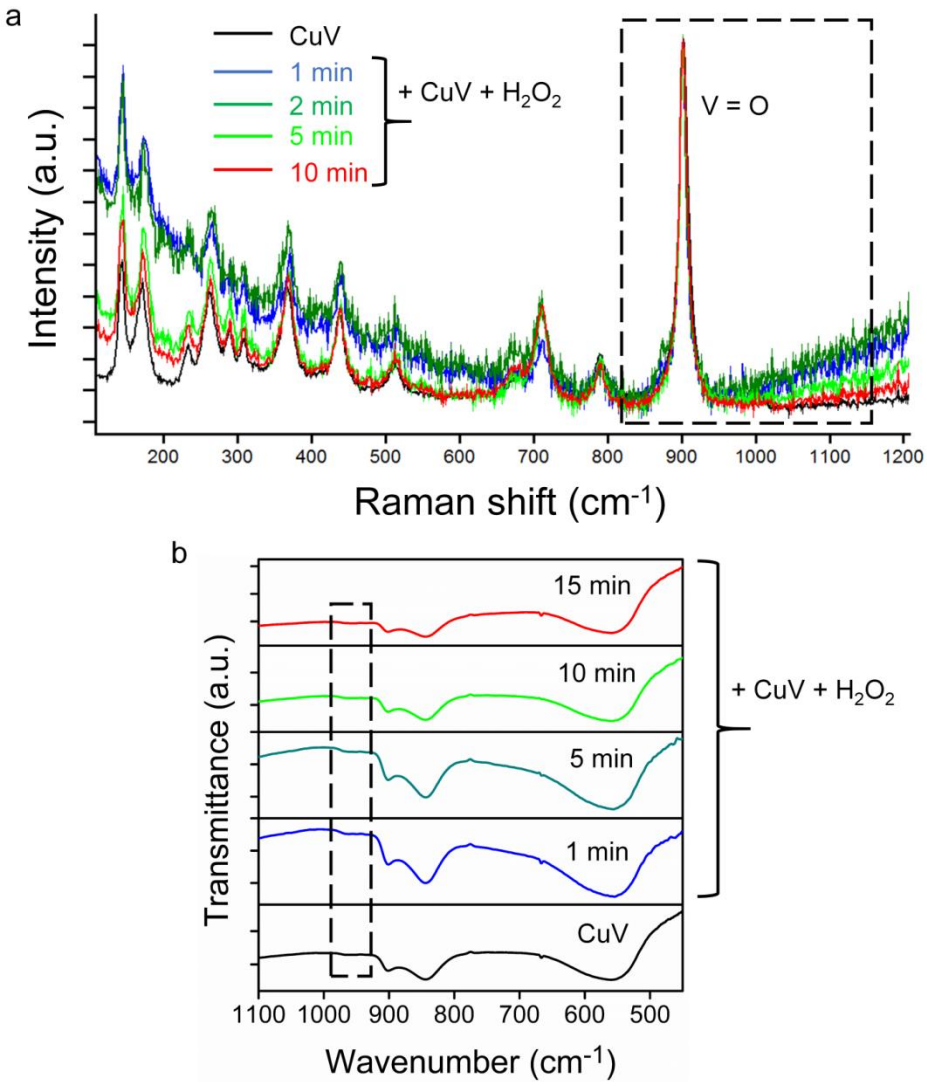

Figure S27. a) Time-dependent FT-Raman spectra of CuV after treatment with 0.1 M H_2O_2. The Peak at 905 cm^{-1} is due to the V=O and after treatment of H_2O_2, no additional peak at 1150 cm^{-1} (V-peroxido) was observed. It was also observed that the peak intensity of V=O was not decreased with time indicated there was no formation of V-peroxido species on the surface of CuV unlike VNw reported in previous literature.[15,22] b) Time-dependent FT-IR spectra of CuV after treatment with 0.1 M H_2O_2. Similar to FT-Raman spectra, there was no peak observed at 930-940 cm^{-1}, characteristic of V-peroxido species[18,26] indicated no formation of V-peroxido on the surface of CuV.

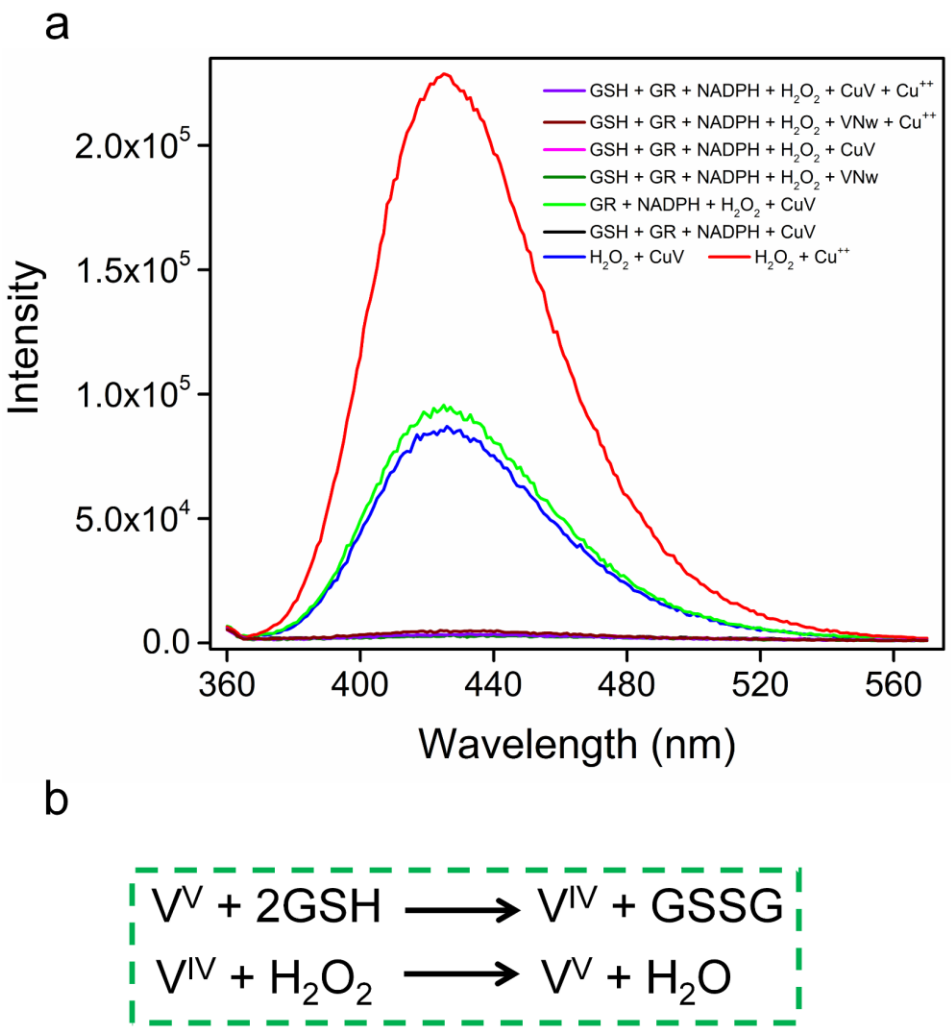

Figure S28. a) Detection of hydroxyl radicals by using terephthalic acid (TPA) (1.0 mM) to produce 2-hydroxyterephthalic acid, which displays a fluorescence emission peak at 425 nm with excitation at 320 nm. TPA was dissolved in basic medium and used for assay in 0.1 M sodium phosphate buffer medium, pH 7.4. The constituents were H_2O_2 (10 mM), NADPH (0.2 mM), GSH (2.0 mM), GR (~1.7 U). Fluorescence spectra were recorded at different assay conditions to check whether CuV (20 ng.µL^{-1}) generate hydroxyl radicals. Along with CuV, Cu^{2+} (20 µM) and VNw (20 ng.µL^{-1}) were used as control. It was noticed that CuV could not generate hydroxyl radicals when all the constituents were present necessary for GPx-like activity. Even in presence of Cu^{2+} both CuV and VNw could not produce hydroxyl radicals. But, without one or more constituents, CuV could generate hydroxyl radicals like Cu^{2+} upon reaction with H_2O_2 which indicates CuV followed a catalytic mechanism to scavenge hydroxyl radicals. B) Schematic of the catalytic mechanism of GPx-like activity on the surface of CuV through redox change of vanadium center.

References

[1] H. Ma, S. Zhang, W. Ji, Z. Tao and J. Chen, *J. Am. Chem. Soc*., 2008, **130**, 5361.

[2] Y. Sun, C. Li, L. Wang, Y. Wang, X. Ma, P. Maa and M. Song, *RSC Advances,* 2012, **2**, 8110.

[3] Q. Zhang, K. Zhang, D. Xu, G. Yang, H. Huang, F. Nie, C. Liu and S. Yang, *Prog. Mater. Sci.,* 2014, **60**, 208.

[4] M. Sabbaghann, J. Beheshtian and R. N. Liarjdame, *Mater. Lett*., 2015, **153**, 1.

[5] T. W. Hart, *Tetrahedron Lett.,* 1985, **26**, 2013.

[6] L. H. Pignolet, R. A. Lewis and R. H. Holm, *J. Am. Chem. Soc.,* 1971, **93**, 360.

[7] A. J. P. Cardenas, R. Abelman and T. H. Warren, *Chem. Commun.,* 2014, **50**, 168.

[8] N. Singh, M. A. Savanur, S. Srivastava, P. D'Silva and G. Mugesh, *Angew. Chem. Int. Ed.,* 2017, **56**, 14267.

[9] M. P. Gordge, J. S. Hothersall and A. A. Noronha-Dutra, *Br. J. Pharmacol.,* 1998, **124**, 141.

[10] S. Ghosh, P. Roy, S. Prasad and G. Mugesh, *Chem. Sci.*, 2019, **10**, 5308.

[11] Y. Wei, C. W. Ryu, G. Chen and K. B. Kim, *Electrochem. Solid-State Lett*., 2006, **9**, A487.

[12] P. F. Newhouse, D. A. Boyd, A. Shinde, D. Guevarra, L. Zhou, E. Soedarmadji, G. Li, J. B. Neatoncd and J. M. Gregoire, *J. Mater. Chem. A,* 2016, **4**, 7483.

[13] C. J. Patridge, C. Jaye, H. Zhang, A. C. Marschilok, D. A. Fischer, E. S. Takeuchi and S. Banerjee, *Inorg. Chem*., 2009, **48**, 3145.

[14] S. Poulston, P. M. Parlett, P. Stone and M. Bowker, *Surf. Interface Anal.,*1996, **24**, 811.

[15] M. C. Biesinger, L. W. M. Laua; A. R. Gerson and R. C. Smart, *Appl Surf Sci*., 2010, **257**, 887.

[16] A. Sahai, N. Goswami, S. D. Kaushik and S. Tripathi, *Appl. Surf. Sci.,* 2016, **390**, 974.

[17] Y. Deng, A. D. Handoko, Y. Du, S. Xi and B. S. Yeo, *ACS Catal.,* 2016, **6**, 2473.

[18] S. Ghosh, P. Roy, N. Karmodak, E. D. Jemmis and G. Mugesh, *Angew. Chem. Int. Ed.,* 2018, **130**, 4600.

[19] A. V. Peskin and C. C. Winterbourn, *Clin. Chim. Acta,* 2000, **293**, 157.

[20] N. Singh, M. A. Savanur, S. Srivastava, P. D'Silva and G. Mugesh, *Angew. Chem. Int. Ed.,* 2017, **56**, 14267.

[21] S. Kundu, W. Y. Kim, J. A. Bertke and T. H. Warren, *J. Am. Chem. Soc.,* 2017, **139**, 1045.

[22] S. Zhang, N. Çelebi-¨Olç¨um, M. M. Melzer, K. N. Houk and T. H. Warren, *J. Am. Chem. Soc*., 2013, **135**, 16746.

[23] Y. Ju-Nam, Y. S. Chen, J. J. Ojeda, D. W. Allen, N. A. Cross, P. H. E. Gardiner and N. Bricklebank, *RSC Adv*., 2012, **2**, 10345.

[24] E. Hryha, E. Rutqvist and L. Nyborg, *Surf. Interface Anal.,* 2012, **44**, 1022.

[25] J. E. Molinari and I. E. Wachs, *J. Am. Chem. Soc.,* 2010, **132**, 12559.

[26] C. Djordjevic, N. Vuletic, M. L. Renslo, B. C. Puryear and R. Alimard, *Mol. Cell. Biochem.,* 1995, **153**, 25.

[27] C. Hao, A. Qu, L. Xu, M. Sun, H. Zhang, C. Xu and H. Kuang, *J. Am. Chem. Soc.,* 2019, **141**, 1091.